

CrystEngComm

Accepted Manuscript



This is an *Accepted Manuscript*, which has been through the Royal Society of Chemistry peer review process and has been accepted for publication.

Accepted Manuscripts are published online shortly after acceptance, before technical editing, formatting and proof reading. Using this free service, authors can make their results available to the community, in citable form, before we publish the edited article. We will replace this *Accepted Manuscript* with the edited and formatted *Advance Article* as soon as it is available.

You can find more information about *Accepted Manuscripts* in the [Information for Authors](#).

Please note that technical editing may introduce minor changes to the text and/or graphics, which may alter content. The journal's standard [Terms & Conditions](#) and the [Ethical guidelines](#) still apply. In no event shall the Royal Society of Chemistry be held responsible for any errors or omissions in this *Accepted Manuscript* or any consequences arising from the use of any information it contains.

Tuning the size and shape of nano-boehmites by a free-additive hydrothermal method

Pablo Pardo, Noemí Montoya and Javier Alarcón

University of Valencia, Department of Inorganic Chemistry, Calle Doctor Moliner 50, 46100-Burjasot
(Valencia), Spain

1. Introduction

The preparation of boehmite nanoparticles in aqueous solution and its further structural and microstructural characterization, including the stability of their aqueous colloidal dispersions, has received considerable attention during last decades¹⁻⁴. The interest in this aluminum oxyhydroxide has been raising in the last few years because its outstanding properties allow a wide number of applications in such different fields as ceramic coating, catalysts or sensors for aqueous solution^{5, 6}. Thus, different alumina oxides, from γ -Al₂O₃ to α -Al₂O₃, are obtained from γ -AlOOH - i. e. boehmite^{7, 8}- and often used as support for catalyzers. Recently, our group reported some results on cation and anion sensing and potential contrast agents of some amine molecules grafted on boehmite nanoparticle supports⁹⁻¹². It is to note that for many of the current applications of boehmite nanoparticles not only is needed to control the size and morphology of particles but also it is crucial to achieve long time stability of their aqueous dispersion^{13, 14}.

Three main routes have been generally used for the preparation of boehmite nanoparticles. One of them is by hydrolysis and condensation of aluminum alkoxides under ambient conditions and its further peptization. Most of the functionalized boehmite nanoparticles used in several applications were synthesized by using this route^{15, 16}. Also, the precipitation of inorganic salts under ambient conditions was a common method, being the main drawback the required control of several experimental reaction parameters^{17, 18}. On the contrary, the preparation of boehmite through the hydrothermal route can be reached under a very wide range of synthetic conditions¹⁹⁻²². Broadly speaking, the morphology of boehmite nanocrystals prepared by the hydrothermal route is strongly dependent on the pH of precipitation of the aluminum hydroxide or oxohydroxide at the first step, i. e. before the hydrothermal processing. Under an initial pH<5 boehmite crystallized as fibers whereas under pH>10 the obtained boehmite were plate-like crystals. Remarkably, most of the reported morphologies obtained in the preparation of boehmite under hydrothermal conditions were acicular^{23, 24} and only very few were plate-like crystals²⁵.

The experimental reaction parameters usually considered in the preparation of boehmite nanoparticles under hydrothermal conditions are the initial pH and the temperature and time of the hydrothermal processing. However, according to some authors the precipitation temperature of aluminum oxohydroxide/hydroxide

(xerogel) from the initial aluminum solution at the first step is also important^{1, 15}, so it will also be considered in the present work. Furthermore, as it has been evidenced by recent reports on the morphology control of nanostructured boehmite under steam treatment, the morphology of resulting nanomaterials is dependent also on the water/gel ratio applied²⁶. In the so-called steam treatment, the required amount of water is poured at the bottom of the PTFE vessel and physically separated from the xerogels. In this work, a simplification of this methodology is proposed, discarding the physical separation between the water and the gel. It seems reasonable to assume that the variation of the water/xerogel ratio for a given temperature and time of hydrothermal processing, in which the xerogel and the required amount of water are in contact inside the PTFE vessel, must also influence the morphology and size of final boehmite.

The present paper intends to determine the effect that the water/solid (xerogel) ratio variation has on the size, morphology and aqueous dispersion colloidal stability of boehmites prepared by hydrothermal processing. Xerogels were firstly obtained by precipitation and then hydrothermally aged with different proportions of water. Our main goal would be to outline the possibility of having a route of tailor-made free-additive boehmite nanoparticles with the desired sizes and morphologies and longtime stability in aqueous dispersion.

2. Experimental section

2.1. Preparation procedure

Materials were prepared following a two-step method. First, an amorphous xerogel was obtained after drying the precipitate formed when the pH of an aluminum salt solution was increased. The second step consisted in the hydrothermal treatment of the xerogel to obtain crystalline nanoparticulated boehmite.

A set of 12 materials was prepared by combination of two different precipitation pHs (5 and 10) and temperature values (25 and 100 °C) for the first step, with three different water/xerogel ratios (1/1, 6/1 and 15/1) used in the subsequent hydrothermal treatment. Reagents were used as received.

More specifically, an initial 0.8 M $\text{Al}(\text{NO}_3)_3 \cdot 9\text{H}_2\text{O}$ (Panreac) solution was heated to 100 °C under stirring in a reflux system or simply stirred at 25 °C. Once the temperature was stabilized, aqueous NH_3 (25%) for acidic and NaOH for alkaline conditions was dropwise added until the pH value was adjusted to 5 or 10 respectively. A white precipitate of boehmite was formed during the addition. The so-obtained precipitate was vacuum filtered, washed and dried overnight at 100 °C to obtain the corresponding xerogels. Hydrothermal aging was subsequently applied to controlled water/xerogel ratios, i.e. 1/1, 6/1 and 15/1. Suspensions were prepared with 1g of xerogel and the corresponding amount of water. Hydrothermal treatment was carried out under autogenous pressure in PTFE lined stainless steel autoclaves placed in a muffle oven at 200 °C for 48 h. The gels were recovered after the treatment and dried overnight at 60 °C.

Xerogels obtained by precipitation at pH 5 and 10 at both temperatures 25 and 100 °C were referred as X(pH)-Y, where X(pH) stands for xerogels (X) precipitated at each pH (5 or 10) and Y corresponds to the temperature of the precipitation (25 or 100 °C). Hydrothermally processed xerogels were labeled X(pH)-Y-R, where R indicates the water/xerogel weight ratio used in the hydrothermal treatment (1/1, 6/1 and 15/1).

2.2. Materials characterization

Transmission electron microscopy (TEM) observations were performed at 100 kV in a Jeol 1010 electron microscope (Tokyo, Japan). Samples were prepared by dispersing the dry powders in water with ultrasonication (150 W, 10 minutes) and setting a drop of the suspensions on copper grids that had previously been coated with a holey thin carbon film. Image J software was used for the size measurements performed on the micrographs and the subsequent data analysis, including the generation of size distributions. Since depending on the experimental conditions of synthetic procedure the morphology developed on the boehmite particles is quite different, from acicular to plate-like nanocrystals, the measured size of nanoparticles correspond to the magnitude of the longer dimension, i.e., the length of acicular particles and the larger diagonal of plate-like crystals. It is to note that the number of particles measured for each sample is between 44 and 226, which allows estimating standard deviations.

HRTEM images and electron diffraction patterns were collected using a Tecnai G2 F20 field emission electron microscope operating at 200 kV and equipped with a Gatan CCD camera. Samples were also prepared by the evaporation of very dilute aqueous suspensions onto carbon-coated grids. Data treatment was performed with Digital Micrograph software.

XRD analysis of powder samples were performed in a Bruker D-8 Advance diffractometer, using $\text{CuK}\alpha$ radiation, with 1 and 3 mm divergence and antiscattering slits respectively and a $3^\circ 2\theta$ range Lynxeye linear detector. The X-ray powder diffraction patterns were run from 5 to $80^\circ 2\theta$ with a step size of $0.02^\circ 2\theta$ and an accumulated counting time of 0.2 s.

Rietveld refinement of calculated diffraction profiles was performed on diffractograms acquired from 5 to $120^\circ 2\theta$ with a step size of $0.02^\circ 2\theta$ and an accumulated counting time of 2s. X'Pert Highscore Plus software was used for the profiles' fitting operations. The determination of crystallite size in specific different crystallographic directions, i. e. [100], 010] and [001] was performed by the application of Scherrer's equation after profile analysis of the corresponding XRD pattern with the EVA software.

Surface characterization and colloidal stability of the different materials were evaluated by the determination of ζ -potential in a pH range between 3 and 11 using a Zetasizer Nano ZS (Malvern Instruments) equipment. Aqueous suspensions (0.1 g/L) of the materials prepared by sonication (10 minutes, 150 W) were adjusted to the different pH values with NaOH and HCl and measurements were replicated three times. Particle size distribution were also measured by dynamic light scattering (DLS) with this equipment on sonicated 0.01 g/L suspensions.

3. Results and discussion

3.1. Morphological analysis. TEM and DLS measurements.

Figure 1 displays the TEM images of the complete set of samples. As can be seen, different particle shapes were observed depending on the preparation conditions. From the whole picture it can be inferred that the main reaction parameter determining the final shape of the boehmite nanoparticles was the pH of the

precipitation step. Samples precipitated at pH 5 showed particles with acicular shapes, either longer fibers or shorter rods depending on the precipitation temperature (25 or 100 °C respectively). When the precipitation proceeded at pH 10 platelet-like particles were obtained at both temperatures. The dependence of the shape of boehmite nanoparticles after the hydrothermal processing of the precipitated xerogels on the precipitation pH agrees with previously reported results^{18, 27-30}. In general, regardless of the acid or base used to adjust the precipitation pH, acidic conditions always led to acicular particles, whereas alkaline media produced nanoplatelets. Nevertheless, the analysis of the initial precipitates carried out in the present study allowed to establish that this shape differentiation with pH in boehmites prepared by hydrothermal via was, remarkably, already effective in the xerogels. The precipitation, thus, proceeded favouring a specific morphology of the particles which was further defined during the hydrothermal treatment. This statement can be clearly inferred from the observation of images X5-25, X5-100, X10-25 and X10-100 in Figure 1. Acidic xerogels, were mainly conformed by fibers or rods, and presented a small proportion of platelet-shaped particles that were not detected in the subsequent hydrothermally treated materials. In xerogels obtained in basic media and in their corresponding hydrothermal products just platelet-like nanoparticles were observed.

The effect of the hydrothermal processing of xerogels by steam treatment has been recently reported³¹. In this study the initial xerogel was prepared by precipitation at room temperature of an $\text{Al}(\text{NO}_3)_3 \cdot 9\text{H}_2\text{O}$ by raising its pH with a base until pH 5. The steam treatment carried out, unlike the experimental procedure applied in the present work, avoided the direct contact between water and gel in the hydrothermal aging. This methodological difference led to slightly different results respect to the present work, as the occurrence of platelet-shaped nanoparticles of a trihydrated alumina ($\text{Al}_2\text{O}_3 \cdot 3\text{H}_2\text{O}$) by steam treatment at 200 °C for 48 h with a 1/1 water to gel ratio. However, for other water to gel ratios tested, i.e. 2/1, 4/1 and 6/1, nanoribbons or nanorods were produced, in agreement with this study.

Beyond the morphological analysis, the measurements performed on TEM micrographs of samples prepared in acidic conditions allowed to establish an unreported effect of the water/gel ratio on the length of the boehmite nanoparticles. Through the evaluation of the average length of microfibers and nanorods prepared in acidic conditions it was found that increasing the relative amount of water in the hydrothermal treatment resulted in a noticeable decrease in the length of the final particles. Table 1 summarizes the results of size

measurements on TEM images for all the samples. Large standard deviation values are intrinsic to the methodology; still, the numeric data obtained allowed a better understanding of the evolution of the system. As qualitatively observed, in the acidic procedure, length of fibers precipitated at 25 °C was larger than that of the nanorods produced at 100 °C. The length decrease caused by the higher proportion of water was larger in the sequence X5-25 (321.0 - 140.7 nm) than in samples X5_100 (70.6 - 52.8 nm) over the range of water/xerogel ratios from 1/1 to 1/15. The length distributions calculated from the measurements also reduced their full width at half maximum (FWHM, Table 1) with increasing water-to-solid ratio. Considering the two series of materials, a wide range (ca. 300 to 50 nm) of length-controlled boehmite microfibers and nanorods was prepared.

Size measurements were performed as well in alkaline series X10-25 and X10-100, considering the longer diagonal of the rhombohedral (010) basal surface. Although not as pronounced as in the case of acicular materials, a slight reduction of size for the platelets of samples precipitated in basic conditions was also observed with increasing water/xerogel ratio. Materials obtained from sample X10-100 always showed larger sizes than those of sample X10-25, altogether comprising a range of ca. 50 to 25 nm size platelets.

Interestingly and despite the differences in the physical principle and the determined magnitude of the techniques, results of DLS measurements matched the observations based on TEM image analysis, thus assessing, with much higher statistical significance, the validity of the applied methodology. Figure 2 shows the particle size distributions of samples precipitated under acidic conditions. For the sake of clarity just 1/1 and 15/1 water/solid ratio hydrothermal treatments are shown. As previously determined, samples precipitated at room temperature showed larger sizes than those heated to 100 °C during the precipitation step. The described decrease of particle length with increasing water/solid ratio was also observed by this technique. In Figure 2 the range of sizes (ca. 320-50 nm) where this methodology produced monomodal size distributions of boehmite microfibers or nanorods is clearly shown. As above mentioned, a good agreement between TEM and DLS size distributions was found. This can be verified in the superimposed distributions presented in Figure 3, where a remarkable overlapping can be observed between both techniques. Regarding this match it is important to consider that size values measured by DLS correspond to the hydrodynamic diameter of the particles in suspension, i.e., the diameter of the hypothetical solid sphere that diffuses at the

same speed that the particle. For the case of well-dispersed boehmite particles of acicular shape this magnitude had a good correspondence to their mayor length, which was measured on the projected image of the particles obtained in TEM observations. Commonly a number of factors affect either DLS or TEM size determinations, preventing the agreement in absolute values between their respective results. The correspondence found in this work for the acid-precipitated boehmite particles sustained two considerations: first, it proved the suitable water dispersability of the material, enough to allow the measurement of primary particles by DLS. Second, it validated the results obtained with the accumulation of measurements on TEM images. On the other hand, for samples precipitated at pH 10, the 2D platelet-like morphology increased the mismatching between the hydrodynamic diameter and any real dimension of the particle. This, together with a lower dispersability, impeded the agreement between both techniques, leading to an overestimation of sizes through DLS that can be observed in figure 1S. Similar dispersion issues have been previously found in studies applying DLS size determinations^{22,32}.

3.2. Microstructural study of the as-prepared and hydrothermally processed xerogels.

With the aim of understanding the transformations taking place during the hydrothermal aging, a microstructural study of the as-prepared and aged xerogels was performed. This study intends to evaluate the degree of crystallinity of the xerogels and its evolution through the hydrothermal processing to the final nano-boehmites.

Regarding the crystallinity it is interesting to compare the XRD traces of the four xerogels shown in Figure 4. On the one hand, broad, low-intensity reflections corresponding to boehmite crystalline phase are observed in alkaline xerogels (X10), with slightly better definition of the peaks when the precipitation occurred at high temperature, i.e. 100 °C. A noticeable feature in both patterns was the shift of the (020) reflection towards lower angle values ($^{\circ}2\theta$). This effect has been reported to increase with the broadening of the diffraction peak, reaching values of shift of $2^{\circ}2\theta$ with breadths exceeding $5^{\circ}2\theta$ ³³. In our case, shifts of ca. $1^{\circ}2\theta$ are coupled with breadths of $2^{\circ}2\theta$, characteristic values of a boehmite of low crystallinity degree. On the other hand, the formation of crystalline domains of boehmite in acidic precipitation was strongly

hindered, especially when working at 25 °C. The diffraction pattern of sample X-25 clearly evidenced the practical absence of coherent diffraction domains. As it was previously reported¹⁹ an amorphous gel of low solubility is formed when the precipitation is carried out at pH 5 over the temperature range between 20 to 80 °C. Noticeably, in the xerogel prepared at 100 °C it was possible to distinguish broad reflections associated with poorly crystallized domains of boehmite, as shown in the pattern X5-100 in figure 4. To the best of our knowledge, the preparation, under acidic conditions, of a boehmite xerogel with a certain degree of crystallinity evidenced by its corresponding XRD pattern has not been reported so far, as previous works^{26, 31, 32, 34} have always described completely amorphous materials.

The effect of the hydrothermal aging on the crystallinity of the xerogels is shown in Figure 2S. The simple visual inspection of the diffraction patterns allowed inferring that the crystallinity increased dramatically during aging. In order to get a quantitative estimation of the crystallinity of the hydrothermally aged xerogels, the averaged crystallite sizes (D_v) values were obtained by the Rietveld refinement of the diffraction pattern. Table 2 summarizes the averaged crystallite size values for all the final boehmites. The weighted residual (Rwp) values were in the range of those reported in the literature³⁵. As can be seen in table 2, the averaged values of crystallite size for the obtained boehmites were in the range of 11.5 to 23.0 nm. These values differed from the ones estimated by the measurement of the particle dimensions on TEM images. This disagreement could be justified by the highly anisotropic morphologies observed by electron microscopy, taking into account that the D_v values obtained from XRD pattern simulation represent a crystallite equivalent spherical diameter. Furthermore, the possibility of the boehmite nanoparticles being composed by a number of crystallites needs also to be considered among the reasons for this disagreement.

To check the possible anisotropy of the diffraction domains, a single-line analysis of crystallite size in the directions of the crystallographic axis were performed. The results obtained by the application of the Scherrer equation to (020), (200) and (002) reflections as independent single-lines are included in Table 2. Directions [010] and [001] showed crystallite sizes close to the mean value obtained by the Rietveld method, and quite homogeneous along the samples series, with the exception of X10-100-1/1 & 6/1. Direction [100], on the contrary, presented size values noticeable different either to the averaged size or to those of [010] and [001] directions. Of special signification resulted the values of samples X5, which showed the larger sizes

along [100] direction. This elongation of the domains occurred in parallel to that of the particles, previously mentioned in the morphological study. In particular, a good agreement between $D_{V[200]}$ and the particle lengths measured on TEM images for the set X5-100 was found. On the contrary, a large disagreement was observed between these $D_{V(200)}$ and L , in table 2 and 1, respectively. This discrepancy must be associated with the limitations of the applicability of Scherrer's equation³⁶.

High magnification conventional TEM images revealed that the aciculae in acidic xerogels were composed by the aggregation of smaller particles, as can be noticed for both samples in Figure 5. Together with more defined fibers, arrangements of platelet-like nanoparticles under 10 nm in size conformed the elongated shapes of the particles in formation in the gel. In order to retrieve more information about the crystallization process taking place during hydrothermal aging, both, xerogels and final materials were studied by HRTEM. Figure 6A shows fibers and portions of amorphous material in the as-prepared xerogel X5-25. The corresponding electron diffraction image showed elongated, poorly defined poles, characteristic of polycrystalline materials composed by several small coherent diffracting domains. Contrasting with this microstructure, the sample X5-25-1/1, in Figure 6B, showed well defined fibers with no trace of amorphous portion and clearly visible lattice planes in their full length. A single particle of sample X5-25-15/1 of ca. 150 nm length is depicted in figure 6C. The electron diffraction pattern presented in the inset, with punctual, well-defined poles, suggest that the material, in comparison with the xerogel, consisted of monocrystalline nanoparticles which diffracted coherently the electron beam. Another example of this type of microstructure is presented in figure 6D, where lattice planes in a portion of a rod of sample X5-100-1/1 are clearly visible, together with the corresponding coherent pattern of electron diffraction. Consequently, fibers or rods obtained by hydrothermal aging of acidic xerogels consisted of single crystalline particles with length determined by the precipitation temperature of the xerogel and the water-to-solid ratio used in the aging.

3.3. Surface chemistry and ζ -potential determinations.

In order to check the effect of the experimental synthetic conditions on the surface properties of the boehmites, ζ -potential measurements of aqueous suspensions were performed. Figure 7 shows the pH

dependence of ζ -potential of suspensions of boehmite particles prepared at both precipitation temperatures (25 and 100°C) and pHs (5 and 10) and hydrothermally processed with a 1/1 water/xerogel ratio, as an illustrative example. As can be seen, sample X10-100-1/1 showed the highest isoelectric point (IEP), ca- 9.6. This result is in agreement with previously reported results^{25, 37} that established that boehmite nanoparticles of distinct shapes presented differences in their IEP. This is explained considering that each crystal face has a specific point of zero charge; thus, different crystal shapes, involving different proportions of faces, must also entail different global IEP. Sample X10-100-1/1, with acicular shape, presented the more alkaline IEP. This same sample also showed the sharper slope in the change from positive to negative potentials, minimizing the range of pH with low surface charge values where colloidal stability may be compromised. These higher IEPs found for acicular samples have been attributed to the raise of the proportion of (100) and/or (001) lateral faces²⁵, which is in agreement with the microstructural observations. Likewise, the lower values of IEP found for the platelet-shaped particles were also consistent with the expected: (010) basal planes, predominant in this morphology, do not exhibit acid-base properties^{18, 38}, consequently only lateral faces, with less exposed face area, contribute to IEP of the material.

3.4. Comments on the growth mechanism and morphological development

At this point, some discussion on the mechanism of formation of final boehmites by hydrothermal aging of the xerogels is noteworthy. The first point to understand is obviously the different crystallinity and morphological characteristics of the different xerogels prepared. From XRD results of xerogels shown in Fig. 3, it was observed that after precipitation at pH=10 the only aluminum-containing crystalline phase detected in both xerogels was boehmite; however, at acidic pH of 5 the formation of boehmite depended on the temperature of precipitation: while at 100 °C weak boehmite reflections could be observed, at 25 °C no peaks were distinguished in the XRD pattern. From the conventional TEM micrographs of xerogels precipitated at basic pH the presence of primary pseudo-crystalline nanoparticles with sizes in the range of 20 to 50 nm was confirmed (Figure 3S). On the contrary, poorly crystalline rods or amorphous fibers, ranging from 100 to 500 nm were obtained at acidic pH (Figure 4S). In agreement with previous observations¹⁹, alkaline medium favored obtaining discrete boehmite nanoparticles while acidic conditions

yielded a non-crystalline gel. This gel consisted in aciculae formed by the aggregation of smaller particles (10 nm). A previous work³⁹ described similar particle arrangements in a thermolysis process carried out at pH 4-5. This process, consisting in heating an Al^{3+} solution up to 95 °C for one week at constant pH, is very similar to the precipitation step of the present work, only differing in the treatment time. According to the authors, such a procedure allowed to carry out the hydrolysis homogeneously and in conditions close to the thermodynamic equilibrium. The comparatively short time used in this study (2 h.) allowed the observation of the ongoing arrangement of particles into the fibers or rods.

In the same work authors established that acidity and ionic strength act on protonation-deprotonation equilibria of the hydroxyl groups of the surfaces, thus changing the electrostatic surface charge and the chemical composition of the interface. These changes induce modifications on the interfacial tension (γ); when the conditions allow its lowering, the contribution to the free enthalpy of the formation of particles is also lowered, allowing the increase in the system surface area and, consequently, the reduction in the particle size. Not all the crystal faces present the same interfacial tension. Interestingly, in the case of boehmite, faces (101) and (100) show the highest values of γ over the pH range from 4 to 12¹⁸, with a maximum energy density gap respect to (001) and (010) faces at pH 4-5. If the acid-base and ionic strength equilibria with the media help in the stabilization of the later pair of faces, it is assumable to consider that, in an arrangement of particles, it would be energetically favorable that the former faces, i.e. (101) and (100) remain unexposed. On the other hand, the energy density gap is considerably reduced at pH 10, where, besides, γ is close to the maximum for all faces. These conditions could reasonably lead to the development of bigger, non-aggregated platelet-like particles as those observed in alkaline xerogels.

From the starting point of the described xerogels, hydrothermal treatment increased their crystallinity without changing their fundamental morphology. Since solubility of the xerogels in the aging conditions was very low¹⁹ the redissolution-recrystallization process was severely hindered, as no efficient transport of matter was possible with the low concentration of soluble species in equilibrium with the solid. Crystallization, thus, occurred through an in situ solid state transformation involving diffusion of ions within the solid. This mechanism is compatible with the unmodified shapes observed in the final materials. Furthermore, considering the above mentioned model of aggregation of particles to form fibers in the acidic

xerogel, a crystallization of such an arrangement would lead to a single crystal elongated in the [100] direction, as observed in the microstructural characterization of X5 samples and schematized in Figure 8. The increase in the treatment pressure induced by the increment of the water/xerogel ratio determined the final size of the particles, either the mayor diagonal of the platelets or the length of the rods or fibers which, eventually, could brake to form smaller particles.

4. Conclusions

A good control of size of boehmite micro and nanoparticles of two different morphologies was achieved through a facile methodology based on hydrothermal treatment. Microfibers or nanorods between ca. 300 and 50 nm of length and nanoplatelets from ca. 50 to 25 nm of mayor basal dimension were prepared. High free-volume percentages used in the synthesis help to keep the simplicity of materials and equipment, easing the potential escalation of the production. The prepared materials, with the dimensional and microstructural control achieved, can be of great interest in the wide range of current applications of boehmite, comprising such different and active fields as biomedicine, environmental chemistry or catalysis, among others. In this sense, the proved optimal dispersability of as-prepared acicular boehmite nanoparticles could result of remarkable applicability.

Additionally, an implemented methodology based on accumulation of measurements on TEM images was found of great convenience in the evaluation of the microstructural evolution of the samples prepared in this work. The agreement achieved with the results obtained from DLS measurements validated its application in the study of these materials.

Acknowledgements

Financial support from the Spanish Ministry of Economy and Competitiveness through project CONSOLIDER INGENIO 2010 CSD2010-00065 is acknowledged.

Technical support from the Servei Central de Suport a l'Investigació Experimental (SCSIE) of the University of Valencia in the application of TEM and XRD techniques is also acknowledged.

References

1. B. E. Yoldas, *J Applied Chem Biotechnol*, 1973, **23**, 803-809.
2. S. Music, D. Dragcevic and S. Popovic, *Mater Lett*, 1995, **24**, 59-64.
3. X. Bokhimi, J. A. Toledo-Antonio, M. L. Guzman-Castillo and F. Hernandez-Beltran, *J Solid State Chem*, 2001, **159**, 32-40.
4. J. Livage, *Catal Today*, 1998, **41**, 3-19.
5. M. Digne, P. Sautet, P. Raybaud, H. Toulhoat and E. Artacho, *J Phys Chem B*, 2002, **106**, 5155-5162.
6. M. Amoura, N. Nassif, C. Roux, J. Livage and T. Coradin, *Chem Commun*, 2007, 4015-4017.
7. C. Pecharroman, I. Sobrados, J. E. Iglesias, T. Gonzalez-Carreno and J. Sanz, *J Phys Chem B*, 1999, **103**, 6160-6170.
8. H. L. Wen and F. S. Yen, *J Cryst Growth*, 2000, **208**, 696-708.
9. R. Aucejo, J. Alarcon, C. Soriano, M. C. Guillem, E. Garcia-Espana and F. Torres, *J Mater Chem*, 2005, **15**, 2920-2927.
10. E. Delgado-Pinar, J. C. Frias, L. J. Jimenez-Borreguero, M. T. Albelda, J. Alarcon and E. Garcia-Espana, *Chem Commun*, 2007, 3392-3394.
11. E. Carbonell, E. Delgado-Pinar, J. Pitarch-Jarque, J. Alarcon and E. Garcia-Espana, *J Phys Chem C*, 2013, **117**, 14325-14331.
12. E. Delgado-Pinar, C. Rotger, A. Costa, M. N. Pina, H. R. Jimenez, J. Alarcon and E. Garcia-Espana, *Chem Commun*, 2012, **48**, 2609-2611.
13. A. Rutenberg, V. V. Vinogradov and D. Avnir, *Chem Commun*, 2013, **49**, 5636-5638.
14. A. R. Auxilio, P. C. Andrews, P. C. Junk, L. Spiccia, D. Neumann, W. Raverty, N. Vanderhoek and J. M. Pringle, *J Mater Chem*, 2008, **18**, 2466-2474.
15. B. E. Yoldas, *Am Ceram Soc Bull*, 1975, **54**, 289-290.
16. M. Nguiefack, A. F. Popa, S. Rossignol and C. Kappenstein, *Phys Chem Chem Phys*, 2003, **5**, 4279-4289.
17. S. Music, D. Dragcevic and S. Popovic, *Mater Lett*, 1999, **40**, 269-274.

18. J. P. Jolivet, C. Froidefond, A. Pottier, C. Chaneac, S. Cassaignon, E. Tronc and P. Euzen, *J Mater Chem*, 2004, **14**, 3281-3288.
19. K. Okada, T. Nagashima, Y. Kameshima, A. Yasumori and T. Tsukada, *J Colloid Interf Sci*, 2002, **253**, 308-314.
20. J. Sanchez-Valente, X. Bokhimi and F. Hernandez, *Langmuir*, 2003, **19**, 3583-3588.
21. T. Tsukada, H. Segawa, A. Yasumori and K. Okada, *J Mater Chem*, 1999, **9**, 549-553.
22. Y. Mathieu, B. Lebeau and V. Valtchev, *Langmuir*, 2007, **23**, 9435-9442.
23. H. Arami, M. Mazloumi, R. Khalifehzadeh and S. K. Sadrnezhad, *J Alloys Comp*, 2008, **461**, 551-554.
24. Y. L. Feng, W. C. Lu, L. M. Zhang, X. H. Bao, B. H. Yue, Y. Iv and X. F. Shang, *Crys Growth Des*, 2008, **8**, 1426-1429.
25. D. Chiche, C. Chaneac, R. Revel and J. P. Jolivet, *Phys Chem Chem Phys*, 2011, **13**, 6241-6248.
26. S. C. Shen, W. K. Ng, Z. Y. Zhong, Y. C. Dong, L. Chia and R. B. H. Tan, *J Am Ceram Soc*, 2009, **92**, 1311-1316.
27. X. Y. Chen, H. S. Huh and S. W. Lee, *Nanotechnology*, 2007, **18**.
28. X. Y. Chen, Z. H. Zhang, X. L. Li and S. W. Lee, *Solid State Commun*, 2008, **145**, 368-373.
29. C. Kaya, J. Y. He, X. Gu and E. G. Butler, *Micropor Mesopor Mat*, 2002, **54**, 37-49.
30. P. D. Santos, A. C. V. Coelho, H. D. Santos and P. K. Kiyohara, *Mater Res-Ibero-Am J*, 2009, **12**, 437-445.
31. S. C. Shen, W. K. Ng, L. S. O. Chia, Y. C. Dong and R. B. H. Tan, *Cryst Growth Des*, 2012, **12**, 4987-4994.
32. Y. Mathieu, S. Rigolet, V. Valtchev and B. Lebeau, *J Phys Chem C*, 2008, **112**, 18384-18392.
33. R. Tettenhorst and D. A. Hofmann, *Clay Clay Miner*, 1980, **28**, 373-380.
34. S. C. Shen, W. K. Ng, Q. Chen, X. T. Zeng and R. B. H. Tan, *Mater Lett*, 2007, **61**, 4280-4282.
35. D. Chiche, M. Digne, R. Revel, C. Chaneac and J. P. Jolivet, *J Phys Chem C*, 2008, **112**, 8524-8533.
36. J. I. Langford and A. J. C. Wilson, *J Appl Cryst*, 1978, **11**, 102-113.
37. D. Chiche, C. Chizallet, O. Durupthy, C. Channeac, R. Revel, P. Raybaud and J. P. Jolivet, *Phys Chem Chem Phys*, 2009, **11**, 11310-11323.

38. P. Raybaud, M. Digne, R. Iftimie, W. Wellens, P. Euzen and H. Toulhoat, *J Catal*, 2001, **201**, 236-246.
39. J. P. Jolivet, S. Cassaignon, C. Chaneac, D. Chiche and E. Tronc, *J Sol-Gel Sci Tech*, 2008, **46**, 299-305.

Figure captions

Figure 1. Representative TEM images of as-prepared boehmite xerogels and hydrothermally treated materials included in this study.

Figure 2. DLS particle size distributions of samples precipitated at acidic conditions (25 and 100 °C) and hydrothermally treated with water/solid ratios of 1/1 and 15/1. (A: X5-25-1/1, B: X5-25-15/1, C: X5-100-1/1, D: X5-100-15/1).

Figure 3. Superimposition of DLS and TEM size distributions obtained for acid-precipitated samples. (A: X5-25-1/1, B: X5-25-15/1, C: X5-100-1/1, D: X5-100-15/1).

Figure 4. XRD patterns of xerogels. Square-ended bars indicate the position and relative intensity of boehmite reflections (Ref. Code: 00-005-0190) Indexes of main reflections are shown. (*) Ammonium nitrate (Ref. Code: 00-001-0809), (+) Sodium nitrate (Ref. Code: 01-089-0310).

Figure 5. High magnification TEM images of acidic xerogels. A: X5-25; B: X5-100. Scale bars are 20 nm in both images.

Figure 6. HRTEM and electron diffraction images of as-prepared and hydrothermally aged samples: A: as-prepared X5-25, scale bar 50 nm. B: X5-25-1/1, scale bar 10 nm. C: X5-25-15/1, scale bar: 20 nm; D: X5-100-1/1 scale bar: 2 nm.

Figure 7. Variation of ζ -potential with pH for samples hydrothermally treated with 1/1 water/solid ratio.

Figure 8. Schematic representation of microstructural changes occurred during hydrothermal aging. Representation of aged particles was reproduced after reference 25.

Tables

Table 1. Size data for boehmites prepared varying pH and temperature of precipitation (**Precip. T**) and water:xerogel weight ratios in the hydrothermal process at 200 °C for 48 h. **L**- average length value; **Std. Dev**- L standard deviation; **Mode**- L frequency maximum; **n**- number of measurements.

Table 2. Crystallite size values calculated from the XRD line-broadening analysis. **Dv**: Averaged crystallite size obtained from pattern simulation with the Rietveld method. **Rwp**: Weighted residual of the fitting. **Dv_[hkl]**: Crystallite size for (hkl) reflection calculated using the Scherrer equation.

Table 1. Size data for boehmites prepared varying pH and temperature of precipitation (**Precip. T**) and water:xerogel weight ratios in the hydrothermal process at 200 °C for 48 h. **L**- average length value; **Std. Dev.**- L standard deviation; **Mode**- L frequency maximum; **n**- number of measurements.

| Sample | pH | Precip. T (°C) | L (nm) | Std. Dev. (nm) | FWHM (nm) | Mode (nm) | n |
|---------------|-----------|--------------------------|------------------|--------------------------|---------------------|---------------------|----------|
| X5-25-1/1 | 5 | 25 | 321.0 | 126.4 | 333.45 | 205.10 | 44 |
| X5-25-6/1 | 5 | 25 | 207.5 | 84.4 | 205.53 | 136.20 | 57 |
| X5-25-15/1 | 5 | 25 | 140.7 | 53.8 | 134.32 | 77.39 | 50 |
| X5-100-1/1 | 5 | 100 | 70.6 | 28.2 | 72.53 | 61.95 | 193 |
| X5-100-6/1 | 5 | 100 | 56.4 | 23.6 | 50.94 | 33.57 | 122 |
| X5-100-15/1 | 5 | 100 | 52.8 | 21.3 | 34.76 | 30.82 | 226 |
| X10-25-1/1 | 10 | 25 | 33.9 | 14.2 | 19.91 | 22.77 | 86 |
| X10-25-6/1 | 10 | 25 | 31.3 | 12.2 | 28.27 | 22.86 | 72 |
| X10-25-15/1 | 10 | 25 | 25.6 | 10.4 | 16.63 | 16.94 | 196 |
| X10-100-1/1 | 10 | 100 | 52.2 | 20.5 | 36.33 | 35.10 | 104 |
| X10-100-6/1 | 10 | 100 | 44.5 | 20.9 | 39.03 | 25.86 | 139 |
| X10-100-15/1 | 10 | 100 | 43.4 | 22.6 | 32.53 | 31.48 | 77 |

Table 2. Crystallite size values calculated from the XRD line-broadening analysis. **Dv**: Averaged crystallite size obtained from pattern simulation with the Rietveld method. **Rwp**: Weighted residual of the fitting. **Dv_[hkl]**: Crystallite size for (hkl) reflection calculated using the Scherrer equation.

| Sample | Dv (nm) | Rwp (%) | Dv ₍₀₂₀₎ (nm) | Dv ₍₀₀₂₎ (nm) | Dv ₍₂₀₀₎ (nm) |
|--------------|---------|---------|--------------------------|--------------------------|--------------------------|
| X5-25-1/1 | 22.1 | 11.9 | 20.7 | 16.1 | 45.9 |
| X5-25-6/1 | 21.0 | 9.4 | 18.4 | 16.7 | 63.6 |
| X5-25-15/1 | 23.0 | 9.0 | 20.8 | 17.0 | 66.8 |
| X5-100-1/1 | 20.7 | 9.8 | 20.1 | 16.4 | 79.8 |
| X5-100-6/1 | 18.2 | 10.3 | 15.2 | 15.6 | 63.6 |
| X5-100-15/1 | 17.6 | 11.2 | 13.8 | 14.3 | 62.8 |
| X10-25-1/1 | 10.6 | 10.8 | 11.9 | 16.1 | 28.7 |
| X10-25-6/1 | 11.5 | 9.5 | 14.1 | 16.5 | 27.8 |
| X10-25-15/1 | 12.0 | 9.8 | 14.7 | 18.7 | 25.4 |
| X10-100-1/1 | 14.9 | 11.3 | 8.4 | 31.9 | 40.6 |
| X10-100-6/1 | 18.4 | 10.7 | 8.7 | 44.4 | 34.5 |
| X10-100-15/1 | 19.6 | 9.6 | 8.7 | 18.6 | 41.9 |

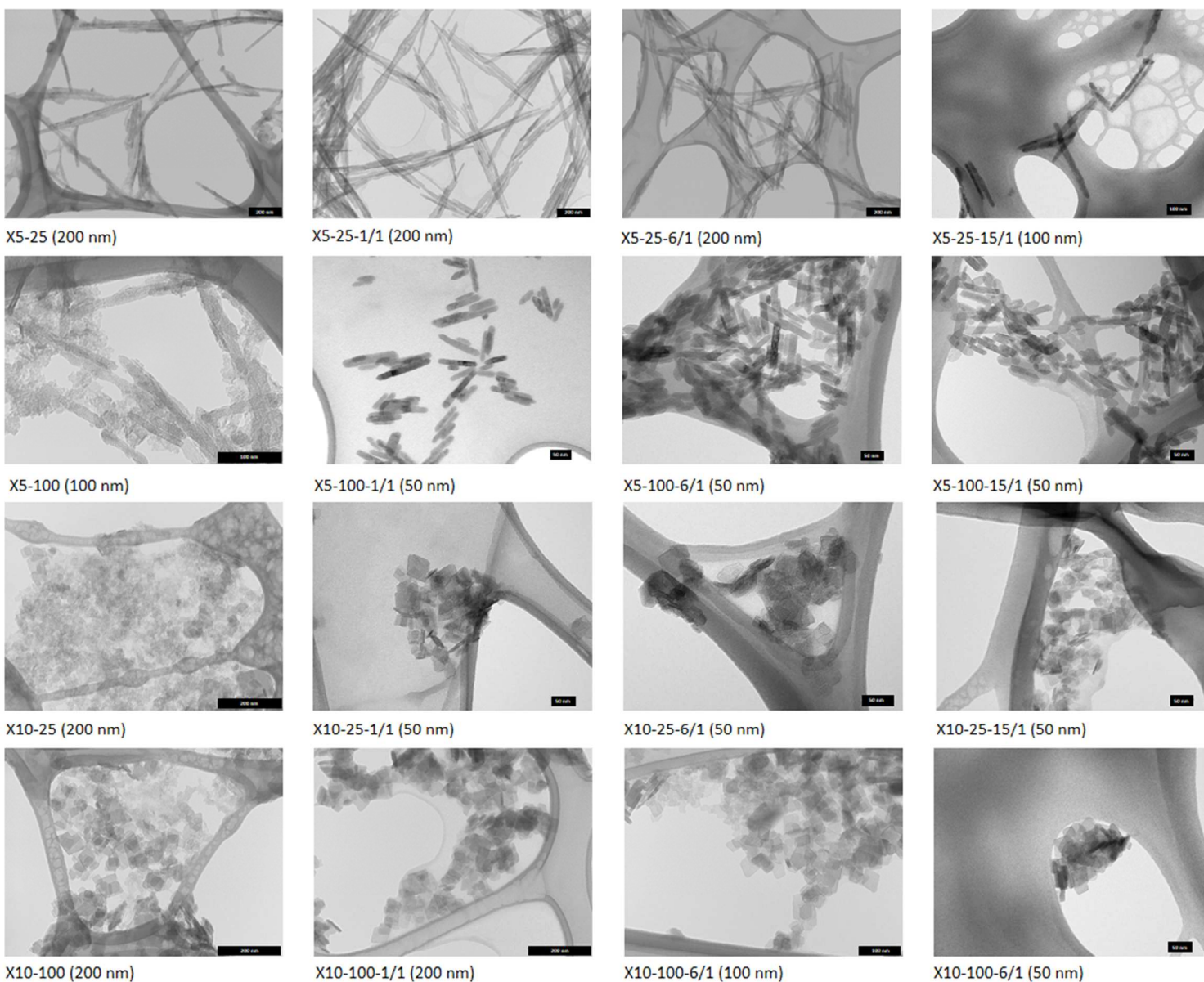


Figure 1. Representative TEM images of as-prepared boehmite xerogels and hydrothermally treated materials included in this study.

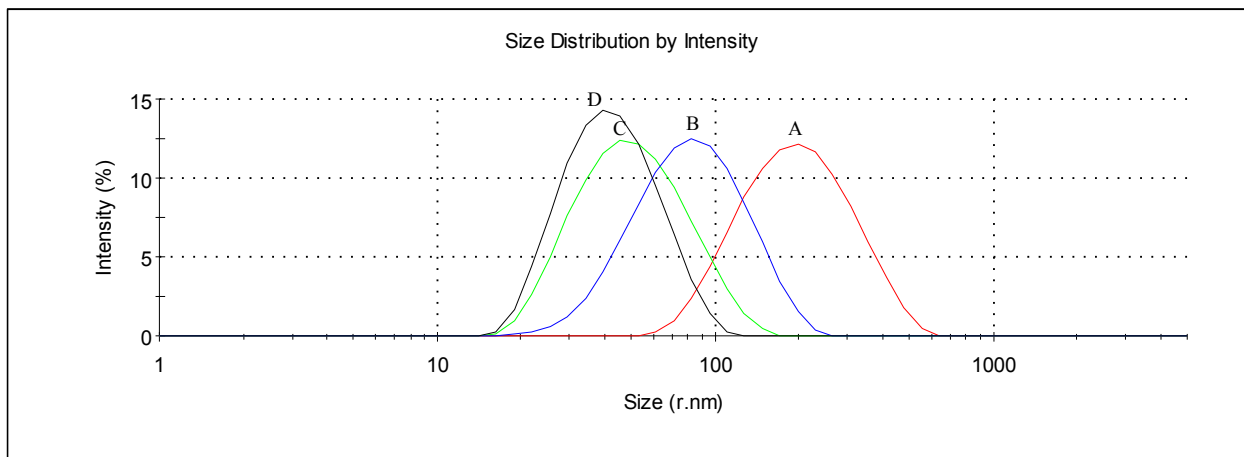


Figure 2. DLS particle size distributions of samples precipitated at acidic conditions (25 and 100 °C) and hydrothermally treated with water/solid ratios of 1/1 and 15/1. (A: X5-25-1/1, B: X5-25-15/1, C: X5-100-1/1, D: X5-100-15/1).

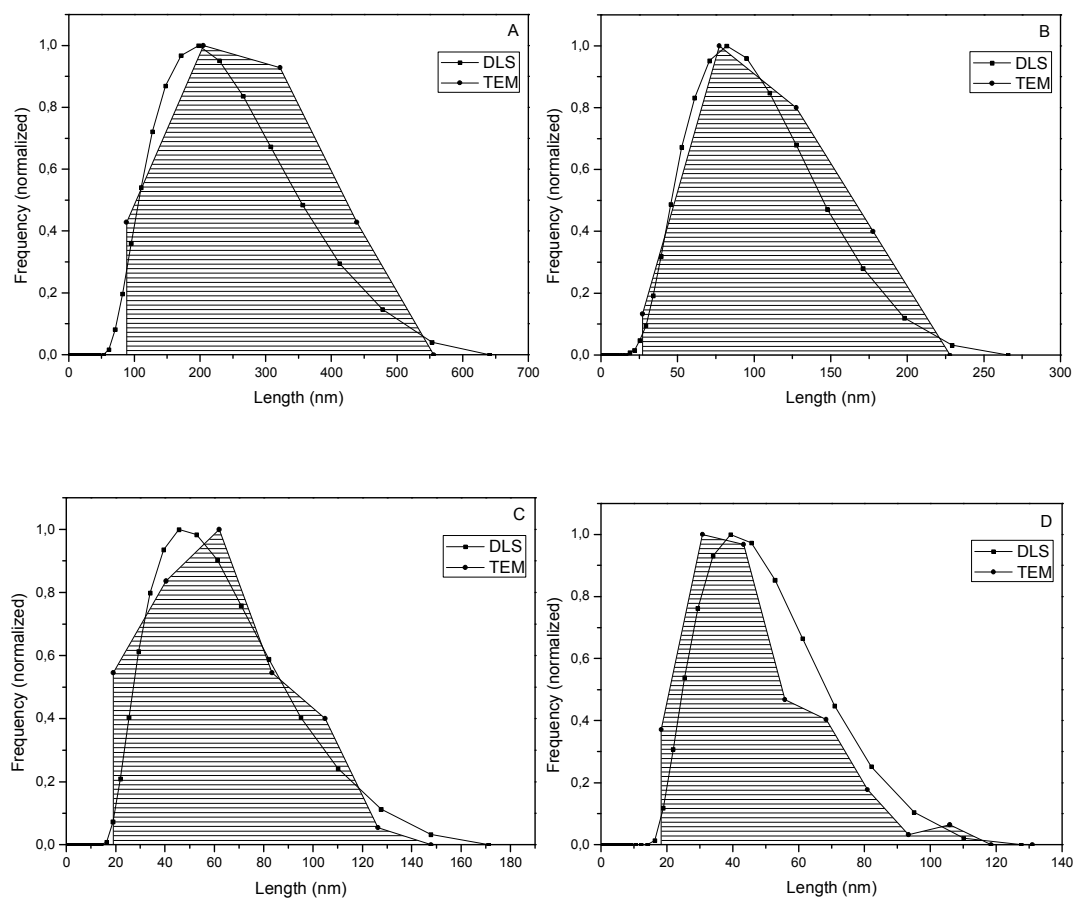


Figure 3. Superimposition of DLS and TEM size distributions obtained for acid-precipitated samples. (A: X5-25-1/1, B: X5-25-15/1, C: X5-100-1/1, D: X5-100-15/1).

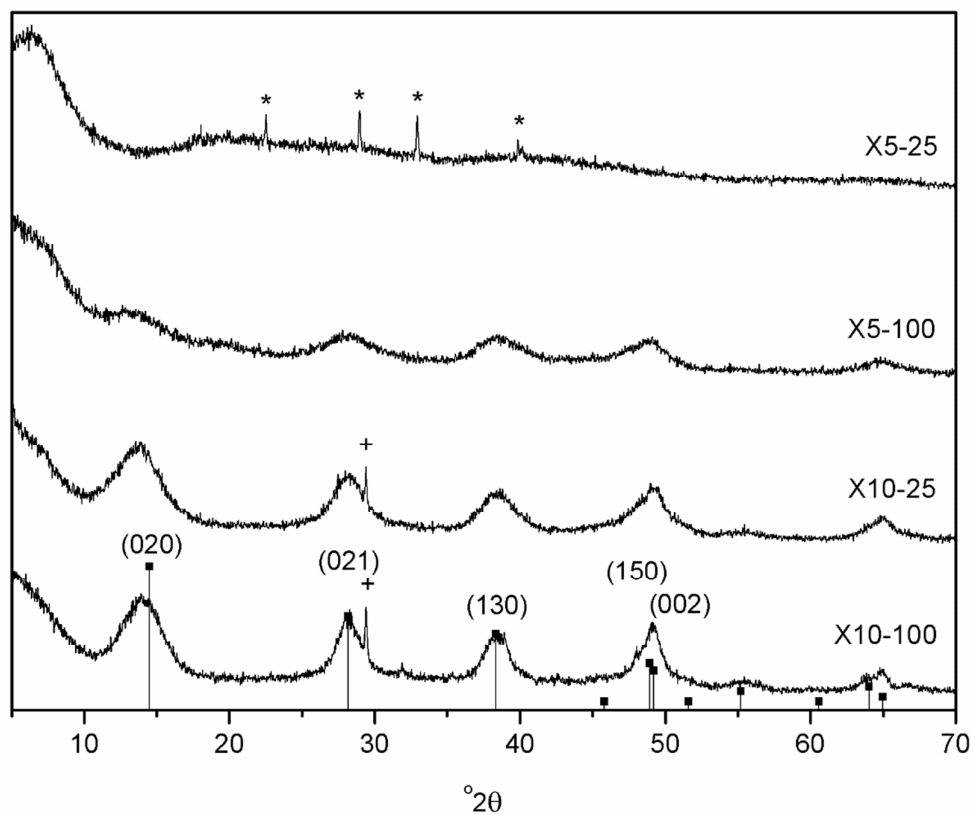


Figure 4. XRD patterns of xerogels. Square-ended bars indicate the position and relative intensity of boehmite reflections (Ref. Code: 00-005-0190) Indexes of main reflections are shown. (*) Ammonium nitrate (Ref. Code: 00-001-0809), (+) Sodium nitrate (Ref. Code: 01-089-0310).

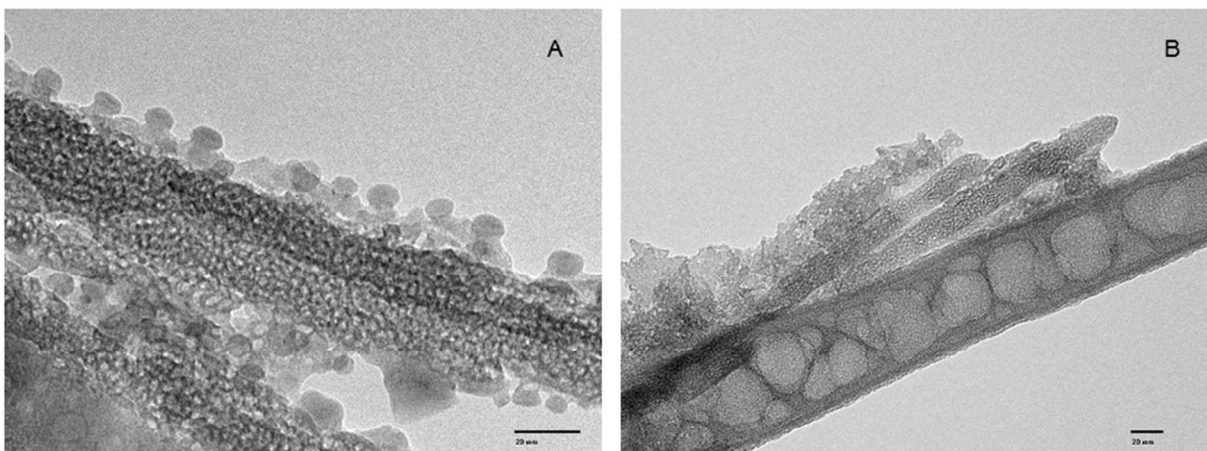


Figure 5. High magnification TEM images of acidic xerogels. A: X5-25; B: X5-100. Scale bars are 20 nm in both images.

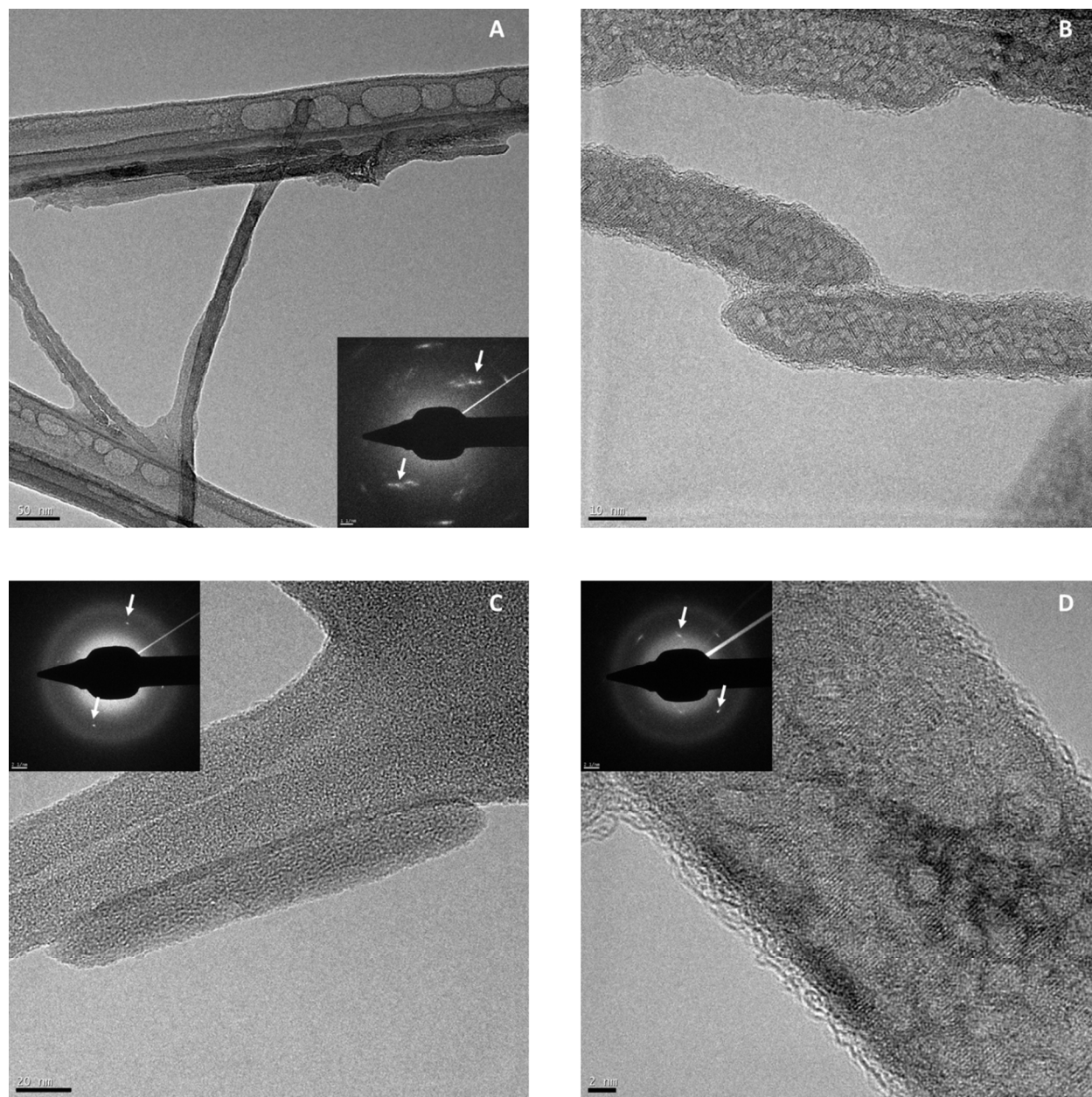


Figure 6. HRTEM and electron diffraction images of as-prepared and hydrothermally aged samples. A: as-prepared X5-25, scale bar 50 nm. B: X5-25-1/1, scale bar 10 nm. C: X5-25-15/1, scale bar: 20 nm; D: X5-100-1/1 scale bar: 2 nm.

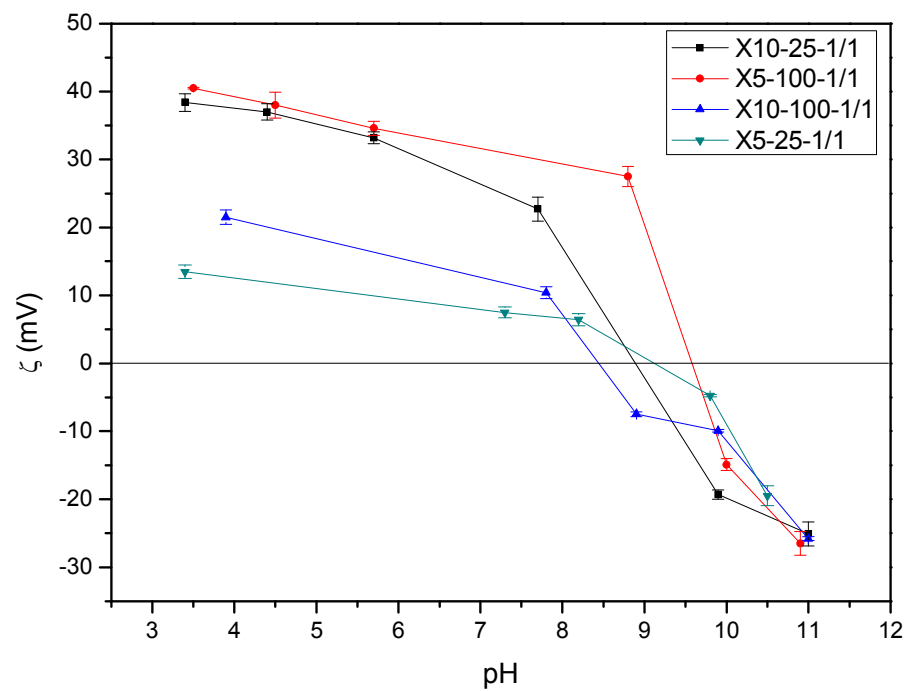


Figure 7. Variation of ζ -potential with pH for samples hydrothermally treated with 1/1 water/solid ratio.

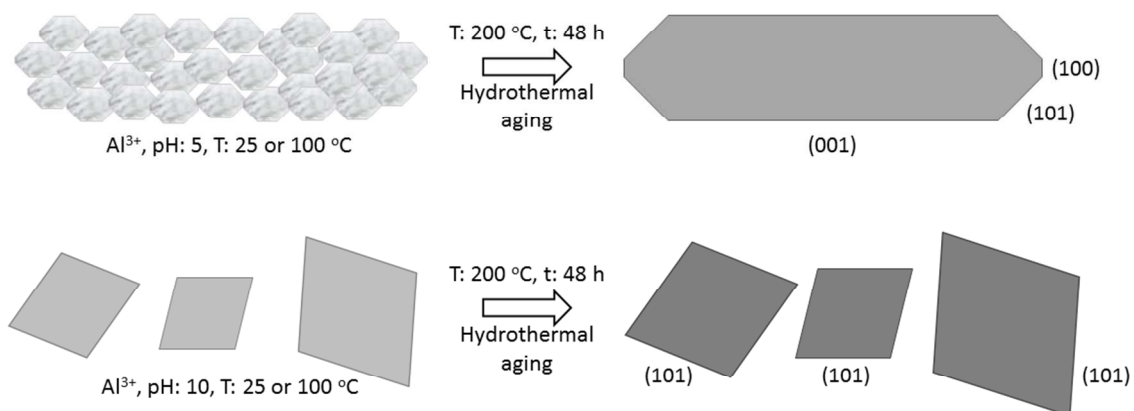
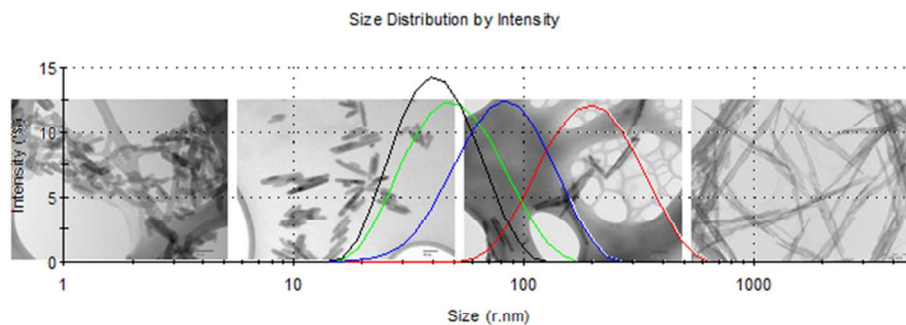


Figure 8. Schematic representation of microstructural changes occurred during hydrothermal aging. Representation of aged particles was reproduced after reference 25.



Nano-boehmites with a range of controlled sizes and morphologies exhibiting high dispersability in water were synthesized through a free-additive hydrothermal methodology.

Nano-boehmites with a range of controlled sizes and morphologies exhibiting high dispersability in water were synthesized through a free-additive hydrothermal methodology
338x190mm (96 x 96 DPI)